Inorganic Chemistry

ARTICLE

pubs.acs.org/IC

Eight-Coordinated Arsenic in the Zintl Phases $RbCd_4As_3$ and $RbZn_4As_3$: Synthesis and Structural Characterization

Hua He, Chauntae Tyson, and Svilen Bobev*

Department of Chemistry and Biochemistry, University of Delaware, Newark, Delaware 19716, United States

Supporting Information

ABSTRACT: Reported are two new series of Zintl phases, ACd_4Pn_3 and AZn_4Pn_3 (A = Na, K, Rb, Cs; Pn = As, P), whose structures feature complex atomic arrangements based on four- and eight-coordinated arsenic and phosphorus. A total of 12 compounds have been synthesized from the corresponding elements via high temperature reactions, and their structures have been established by X-ray diffraction. $RbCd_4As_3$, KCd_4As_3, $NaCd_4As_3$, $NaZn_4As_3$, KCd_4P_3, and KZn_4P_3 crystallize with a new rhombohedral structure (space group $R\bar{3}m$, Z = 3, Pearson symbol $hR24$), while the isoelectronic $RbZn_4As_3$, $CsCd_4As_3$, $CsZn_4As_3$, KZn_4As_3, $CsZn_4P_3$, and $RbZn_4P_3$ adopt the tetragonal KCu_4S_3-type structure (space group $P4/mmm$, Z = 1, Pearson symbol $tP8$). Both structures are very closely related to the ubiquitous $CaAl_2Si_2$ and $ThCr_2Si_2$ structure types, and the corresponding relationships are discussed. The experimental results have been complemented by linear muffin-tin orbital (LMTO) tight-binding band structure calculations. Preliminary transport properties measurements on polycrystalline samples suggest that the compounds of these families could be promising thermoelectric materials.

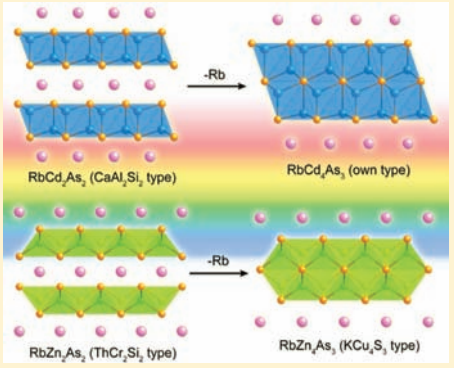

INTRODUCTION

The unprecedented physical properties of several classes of transition metal arsenides and antimonides, discovered in recent years, have captivated the attention of many condensed-matter researchers around the globe.[1−8] Arguably, the renewed interest in the chemistry and physics of ternary and quaternary pnictides is largely due to the discovery of superconductors within the three families of compounds—*RE*OFeAs (ZrCuSiAs type, *RE* = La, Ce, Pr, Nd, Sm),[2] (*A*/*AE*)Fe_2As_2 ($ThCr_2Si_2$ or $CeAl_2Ga_2$ type, *A* = K, Rb, Cs; *AE* = Sr, Ba),[3] and *A*FeAs (PbFCl type, *A* = Li, Na).[4] The promise of some antimonides, e.g., $Yb_{14}MnSb_{11}$,[5] $LaCo_4Sb_{12}$,[6] $Ca_xYb_{1-x}Zn_2Sb_2$,[7] and $EuZn_2Sb_2$,[8] for applications in thermoelectric energy conversion can also be cited as another major contributor to the intense research efforts in this area. The wealth of complicated structures and bonding patterns offered by such compounds (and polar intermetallics in general[9]) also has an appeal from a standpoint of gathering new, fundamental knowledge in the solid state.[10−19]

Our research group has already reported on numerous new pnictides with Zn and Cd, featuring molecular-like $[Cd_4Sb_{12}]^{26-}$ and $[Cd_8Bi_{22}]^{48-}$ fragments, seen in $Ba_{21}Cd_4Sb_{18}$ and $Sr_{21}Cd_4Bi_{18}$;[11] edge-shared tetrahedral $^1_\infty[ZnPn_2]^{4-}$ chains in Ba_2ZnPn_2 (*Pn* = As, Sb, Bi);[12] more intricate $^1_\infty[Cd_6Sb_{12}]^{22-}$/$^1_\infty[Zn_6Sb_{12}]^{22-}$ and $^1_\infty[Cd_4Pn_9]^{19-}$/$^1_\infty[Zn_4Pn_9]^{19-}$ 1D ribbons in $A_{11}Cd_6Sb_{12}$/$Eu_{11}Zn_6Sb_{12}$ (*A* = Sr, Ba, Eu)[13] and $A_9Cd_{4+x}Pn_9$/$A_9Zn_{4+x}Pn_9$ (*A* = Ca, Sr, Eu, Yb; *Pn* = Sb, Bi),[14] respectively; 2D-polyanionic $^2_\infty[CdSb_2]^{4-}$ layers in Ca_2CdSb_2 and Yb_2CdSb_2;[15] $^2_\infty[Cd_2Pn_3]^{4-}$ and $^2_\infty[Cd_2Sb_4]^{6-}$ layers, as in $Ba_2Cd_2Pn_3$ (*Pn* = As, Sb)[16] and $Ba_3Cd_2Sb_4$;[17] and 3D-polyanionic $^3_\infty[Cd_2Sb_3]^{5-}$ networks observed in $KA_2Cd_2Sb_3$ (*A* = Ca, Sr, Ba, Eu, Yb).[18] As seen from above, most of our previous work employed the alkaline-earth metals, and the nominally divalent Eu and Yb metals from the 4*f* block. Having systematically explored the divalent cations, we recently began studying heterovalent systems which include the new families of Zintl phases Na_2ACdSb_2 and K_2ACdSb_2 (*A* = Ca, Sr, Ba, Eu, Yb),[19] as well as the already mentioned $KA_2Cd_2Sb_3$ (*A* = Ca, Sr, Ba, Eu, Yb).[18] Extending the chemistry to compounds based on the alkali metals alone, herein we report on the new layered arsenides AZn_4As_3 and ACd_4As_3 (*A* = Na, K, Rb, Cs), as well as the phosphides $CsZn_4P_3$, $RbZn_4P_3$, KZn_4P_3 and KCd_4P_3. With this paper, we present their crystal structures (two different bonding arrangements containing unusual eight-coordinated pnictogen atoms), established by X-ray diffraction studies, as well as the electronic structures calculated by the LMTO method.[20] For conciseness, $RbCd_4As_3$ and $RbZn_4As_3$ are chosen as examples of the two different structure types, and their crystal chemistry and chemical bonding will be the focus of our attention. The remaining ones are mentioned in the Supporting Information. The close structural relationships between the two newly reported structures and the ubiquitous structures of the $CaAl_2Si_2$ and $ThCr_2Si_2$ families[21] of compounds will also be covered. The results from measurements of the electrical resistivity and Seebeck coefficient on pressed pellets of polycrystalline samples will be discussed as well.

Received: May 5, 2011
Published: August 03, 2011

   dx.doi.org/10.1021/ic2009418 | *Inorg. Chem.* 2011, 50, 8375–8383

EXPERIMENTAL SECTION

Synthesis. All manipulations were performed inside an argon-filled glovebox or under vacuum. The starting materials—pure elements from Alfa or Aldrich (>99.9%)—were used as received. Crystals of $RbZn_4As_3$ and $RbCd_4As_3$ were first identified from reactions aimed at synthesizing pnictide clathrates, analogous to $Cs_8Cd_{18}Sb_{28}$.[22] For this purpose, the corresponding elements Rb, Zn/Cd, and As in a molar ratio of 8:18:28 were loaded into niobium tubes, which were then arc-welded under high purity argon gas. The niobium tubes were subsequently jacketed within fused silica tubes, which were flame-sealed under vacuum. The reaction mixtures were equilibrated at 550 °C for 10 days, then slowly cooled to room temperature at a rate of 5 °C/h. Powder X-ray diffraction patterns of the products of these reactions confirmed $RbZn_4As_3$ and $RbCd_4As_3$ as major phases, along with the clathrate-I $Rb_8Zn_{18}As_{28}$ and $Rb_2Cd_5As_4$[23] as minor phases.

After the structure and the composition of $RbZn_4As_3$ and $RbCd_4As_3$ were established from single-crystal X-ray diffraction work, the reactions were repeated with the correct stoichiometry, yielding the desired compounds as major products. Small amounts of side products—$Rb_8Zn_{18}As_{28}$,[23] $Rb_2Cd_5As_4$,[23] $CdAs_2$,[24] and Zn_3As_2[25]—were still present according to the powder patterns. Attempts to modify the temperature profiles with the idea to optimize the yields included a quick ramp to 850 °C and homogenization at this temperature for 2 h, followed by quenching in icy water. Such heat treatment appeared to help produce essentially phase-pure $RbZn_4As_3$, while the corresponding Cd reaction failed to increase the yield of $RbCd_4As_3$. Instead, $Rb_2Cd_5As_4$ was the major product. Since the crystals of $RbCd_4As_3$ had a distinct golden color, they could be easily separated from the dark-to-black crystals of $Rb_2Cd_5As_4$. In addition, the crystallinity of $RbCd_4As_3$ (as well as of the other rhombohedral phases, *vide infra*) was generally very poor, and annealing steps at 500−600 °C for 7−10 days were necessary to improve the crystal quality.

$CsZn_4As_3$, KZn_4As_3, $NaZn_4As_3$, $CsCd_4As_3$, KCd_4As_3, and $NaCd_4As_3$, as well as four phosphides, $CsZn_4P_3$, $RbZn_4P_3$, KZn_4P_3 and KCd_4P_3, could be synthesized with the above-described synthetic scheme from 1:4:3 stoichiometric mixtures of the corresponding elements. Typically, the compounds that adopt the tetragonal structure could be readily synthesized via fast cooling after homogenizing at high temperature, e.g., 700−850 °C. Li-containing compounds with either structure could not be synthesized, presumably because the Li atoms are much smaller than the rest of the alkali metals.

Caution! *Alkali metals, Rb and Cs especially, react violently with the air, and extreme caution must be exercised when handling these metals. Also, the silica jackets in such reactions should be made sufficiently long, so that one of the ends is left protruding outside the furnace—this must be done for condensation of Rb/Cs vapors in the event of a leak from the niobium ampules into the silica tube.*

Powder X-Ray Diffraction. X-ray powder diffraction patterns were taken at room temperature on a Rigaku MiniFlex powder diffractometer using Cu Kα radiation. The outcome of all reactions and the phase purity was estimated based on the collected diffraction patterns. Since the diffractometer was enclosed in a nitrogen-filled glovebox, we were able to test the air-sensitivity of the title compounds by comparing the diffraction patterns of the freshly prepared samples with those that had been exposed to the air. On the basis of the test results, all of the title compounds are stable in the air for up to two months (a representative powder pattern is provided as Supporting Information).

Single-Crystal X-Ray Diffraction. Single crystals of 11 of the 12 synthesized compounds (except KZn_4As_3) were selected under a microscope. They were cut to suitable dimensions and then mounted on glass fibers using Paratone oil. Intensity data were collected on a Bruker SMART CCD-based diffractometer with monochromated Mo Kα$_1$ radiation (λ = 0.71073 Å). A cold nitrogen stream (200(2) K) was used to maintain a low temperature and immobilize the crystals during the data collections. Full spheres of data were acquired in four batch runs with a frame width of 0.4 or 0.5° for ω and θ. Intensities were extracted and then corrected for Lorentz and polarization effects using the SAINT program.[26] Semiempirical absorption correction based on equivalents was applied using the SADABS code.[27] The structure factors were sorted and merged by the program XPREP, which was also employed in the space group determination. The structures were solved by direct methods and refined to convergence by full matrix least-squares methods on F^2, as implemented in the SHELXTL software.[28] Refined parameters included the scale factor, the atomic positions with anisotropic displacement parameters, and extinction coefficients (where necessary). Standardization of the atomic coordinates before the last refinement cycles was done using STRUCTURE TIDY.[29] Relevant crystallographic data and refinement parameters for $RbZn_4As_3$

Table 1. Selected Crystal Data and Structure Refinement Parameters for $RbCd_4As_3$ and $RbZn_4As_3$, Chosen As Examples of the Two Different Structure Types[a]

empirical formula	$RbCd_4As_3$	$RbZn_4As_3$
fw, g·mol^{-1}	759.83	571.71
space group	$R\bar{3}m$ (No. 166)	$P4/mmm$ (No. 123)
λ, Å	0.71073	
T, K	200(2)	
a, Å	4.4752(10)	4.1714(6)
c, Å	36.946(12)	10.355(3)
V, Å^3	640.8(3)	180.19(6)
Z	3	1
ρ_{calcd}, g·cm^{-3}	5.907	5.269
μ (Mo Kα), cm^{-1}	269.10	334.10
GOF on F^2	1.155	1.221
R_1 [$I > 2\sigma(I)$][b]	0.0212	0.0169
wR_2 [$I > 2\sigma(I)$][b]	0.0442	0.0406

[a] Data for the remaining members of each family are provided as Supporting Information. [b] $R_1 = \Sigma||F_o| - |F_c||/\Sigma|F_o|$; $wR_2 = [\Sigma[w(F_o^2 - F_c^2)^2]/\Sigma[w(F_o^2)^2]]^{1/2}$, and $w = 1/[\sigma^2F_o^2 + (A\cdot P)^2 + B\cdot P]$, $P = (F_o^2 + 2F_c^2)/3$; A and B are weight coefficients. A = 0.0251 for $RbCd_4As_3$; A = 0.0188 for $RbZn_4As_3$; B = 0 for $RbCd_4As_3$; B = 0.155 for $RbZn_4As_3$.

Table 2. Atomic Coordinates and Equivalent Isotropic Displacement Parameters (U_{eq}[b]) for $RbCd_4As_3$ and $RbZn_4As_3$[a]

atom	site	x	y	z	U_{eq} (Å^2)
			$RbCd_4As_3$		
Rb	3*b*	0	0	1/2	0.0160(3)
Cd1	6*c*	0	0	0.08647(2)	0.0165(2)
Cd2	6*c*	0	0	0.30242(2)	0.0202(2)
As1	6*c*	0	0	0.23100(2)	0.0111(2)
As2	3*a*	0	0	0	0.0136(3)
			$RbZn_4As_3$		
Rb	1*b*	0	0	1/2	0.0201(2)
Zn	4*i*	0	1/2	0.15912(5)	0.0153(2)
As1	2*h*	1/2	1/2	0.29233(6)	0.0124(2)
As2	1*a*	0	0	0	0.0119(2)

[a] The refined atomic coordinates for the remaining members of each family are given as Supporting Information. [b] U_{eq} is defined as one-third of the trace of the orthogonalized U^{ij} tensor

dx.doi.org/10.1021/ic2009418 |*Inorg. Chem.* 2011, 50, 8375–8383

Table 3. Important Interatomic Distances (Å) and Angles (deg) in $RbCd_4As_3$ and $RbZn_4As_3$[a]

$RbCd_4As_3$		$RbZn_4As_3$	
distances (Å)			
Cd1−As1 (3×)	2.6494(6)	Zn−As1 (2×)	2.5006(5)
Cd1−As2 (1×)	3.1947(13)	Zn−As2 (2×)	2.6580(5)
Cd2−As1 (1×)	2.6385(14)	As1−Zn (4×)	2.5006(5)
Cd2−As2 (3×)	2.8250(6)	As2−Zn (8×)	2.6580(5)
As1−Cd1 (3×)	2.6494(6)	Rb−As1 (8×)	3.6503(6)
As1−Cd2 (1×)	2.6385(14)	Rb−Zn (8×)	4.1001(9)
As2−Cd1 (2×)	3.1947(13)	Rb−As2 (2×)	5.178(1)
As2−Cd2 (6×)	2.8250(6)		
Rb−As1 (6×)	3.5108(9)		
Rb−Cd1 (6×)	3.9311(10)		
angles (deg)			
As1−Cd1−As1	115.25(2)	As1−Zn−As1	113.04(3)
As1−Cd1−As2	102.78(3)	As1−Zn−As2	110.00(1)
As1−Cd2−As2	113.85(2)	As2−Zn−As2	103.38(2)
As2−Cd2−As2	104.76(2)		

[a] The refined distances for the remaining members of each family are tabulated in the Supporting Information.

(tetragonal structure) and $RbCd_4As_3$ (rhombohedral structure) are summarized in Table 1. Final positional and equivalent isotropic displacement parameters, and selected interatomic distances are listed in Tables 2 and 3, respectively. Details pertaining to the remaining structures are provided as Supporting Information (crystallographic information files, Table S1 and Table S2). CIFs have also been deposited with Fachinformationszentrum Karlsruhe, 76344 Eggenstein-Leopoldshafen, Germany (fax: (49) 7247−808−666; e-mail: crysdata@fiz.karlsruhe.de)—depository numbers CSD-423006 for $RbCd_4As_3$, CSD-423007 for $RbZn_4As_3$, CSD-423008 for $CsCd_4As_3$, CSD-423010 for KCd_4As_3, CSD-422009 for $NaCd_4As_3$, CSD-423011 for $CsZn_4As_3$, CSD-423012 for $NaZn_4As_3$, CSD-423013 for $RbZn_4P_3$, CSD-423014 for KZn_4P_3, CSD-423031 for $CsZn_4P_3$, and CSD-423032 for KCd_4P_3.

Seebeck Coefficient and Resistivity Measurements. Data for only one compound from each series, $NaCd_4As_3$ and $RbZn_4As_3$, which were the phase-purest materials (as judged by powder X-ray diffraction), are presented. Due to the lack of adequate-sized single-crystals, all measurements of the electrical resistivity and Seebeck coefficient were conducted on polycrystalline specimens. For this purpose, polycrystalline powder was cold-pressed into pellets, which were then subjected to annealing (in a vacuum) at 400 °C for 1 week. Rectangular bars were cut from the pellets for both measurements. The resistivity measurement was done with a PPMS system using the four-probe method, and the Seebeck coefficient was measured with a MMR instrument equipped with a K-20 temperature controller and the SB-100 measuring system.

Computational Methodology. Electronic structure calculations were carried out using the tight-binding, linear muffin-tin orbital (TB-LMTO) method,[20] using the Stuttgart TB-LMTO 4.7 package.[30] Local density approximation (LDA) was used to treat exchange and correlation.[31] All relativistic effects except for spin−orbital coupling were taken into account by the scalar relativistic approximation.[32] Discussed herein are the results for $RbCd_4As_3$ and $RbZn_4As_3$, for which the basis set included the 5s, 5p, and 4d orbitals for Rb; 5s, 5p, and 4d orbitals for Cd; 4s, 4p, and 3d orbitals for Zn, ;and 4s, 4p, and 4d orbitals for As. The 5p and 4d orbital of Rb and 4d orbital of As were treated with the downfolding technique.[33] The *k*-space integrations were performed using the tetrahedron method.[34] The Fermi level was set at 0 eV as an energy reference.

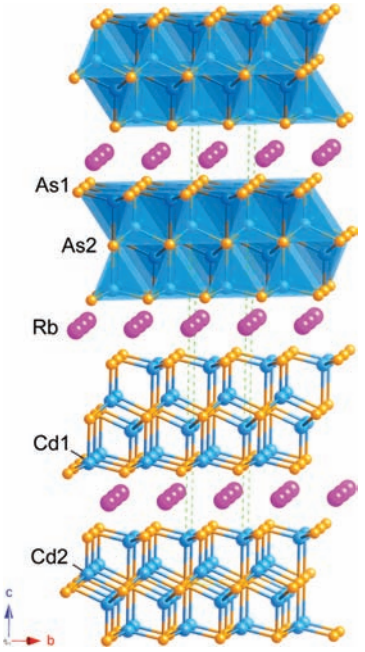

Figure 1. Combined ball-and-stick and polyhedral representations of the crystal structure of $RbCd_4As_3$. Rb atoms are shown as magenta spheres. Cd and As atoms are shown as blue and tangerine spheres, respectively. Cd−As bonds are highlighted, and the unit cell is outlined.

RESULTS AND DISCUSSION

Structures and Phase Relationships. The ternary $RbCd_4As_3$ phase (Figure 1) crystallizes in the centrosymmetric space group $R\bar{3}m$ (No. 166, $Z = 3$). KCd_4As_3, $NaCd_4As_3$, $NaZn_4As_3$, KZn_4P_3, and KCd_4P_3 also form with the same rhombohedral structure. There are five crystallographically unique atoms in the asymmetric unit, all in special positions (Table 2). Formally, the structure can be classified with the Pearson symbol *hR*24;[21] since this atomic arrangement is without a precedent in the Pearson's Handbook, and the latest edition of the Inorganic Crystals Structure Database (ICSD)[35] does not contain known phases with the same space group and Wyckoff letters, $RbCd_4As_3$ is a new structure type.

Figure 1 shows the $RbCd_4As_3$ structure, which can be readily described following the Zintl−Klemm rules[9] as two-dimensional $^2_\infty[Cd_4As_3]^-$ polyanions, made up of fused $CdAs_4$ tetrahedra. These layers are stacked along the *c*-crystallographic direction in a typical *ABCABC* sequence, with layers of Rb^+ cations between them. The $CdAs_4$ tetrahedra are condensed in a complicated pattern, constituting a combination of edge- and corner-sharing.

The polyanionic structure is based on two independent Cd and two independent As atoms (Table 2). Both Cd1 and Cd2 atoms, as indicated above, are tetrahedrally coordinated with As−Cd−As angles very close to 109° (Table 3). The corresponding Cd−As bond distances range from 2.6385(14) to 3.1947(13) Å, whereby the distances in the lower end are only slightly longer than the sum of the Cd and As covalent radii (r_{Cd} = 1.38 Å; r_{As} = 1.21 Å),[36] while at the higher end, they are nearly 20% longer. Such a wide range for the Cd−As contacts

dx.doi.org/10.1021/ic2009418 |*Inorg. Chem.* 2011, 50, 8375–8383

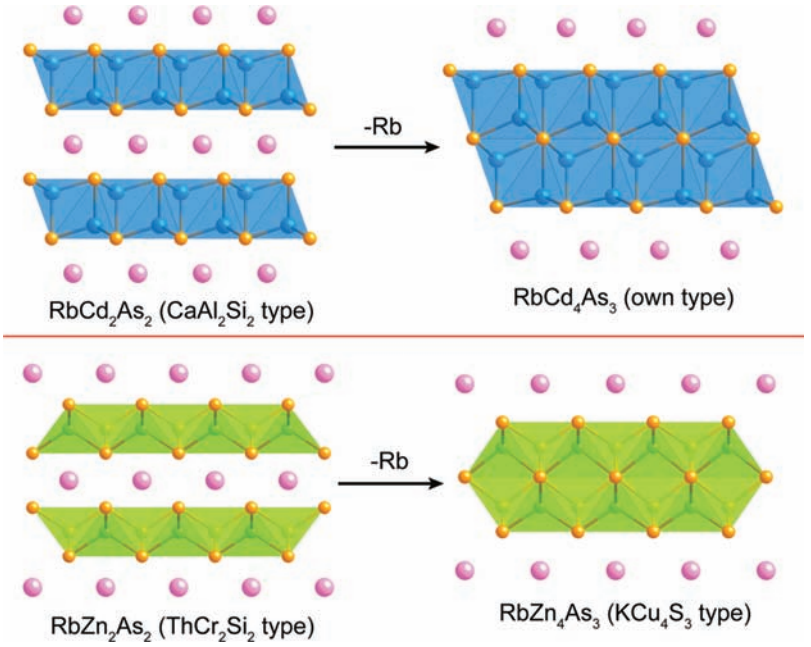

Figure 2. Structural relationship between $RbCd_2As_2$ ($CaAl_2Si_2$ structure type) and $RbCd_4As_3$ and between $RbZn_2As_2$ ($ThCr_2Si_2$ structure type) and $RbZn_4As_3$. See the text for more detail.

indicates a disparity between the Cd−As1 and Cd−As2 bonds. Indeed, this could be easily seen by examining the bonding from the viewpoint of the coordination of As atoms. As1 is at the top and at the bottom of each $^2_\infty[Cd_4As_3]^-$ layer, and it has four nearest Cd neighbors. The coordination environment of As1 is umbrella-shaped, i.e., an inverted tetrahedron, similar to the As atoms in the $^2_\infty[Cd_2As_2]^{2-}$ layers in $CaCd_2As_2$ ($CaAl_2Si_2$ type).[37] The bonding in this arrangement has been previously considered elsewhere; here, we just point out that the As1−Cd2 bonds, which are parallel to the direction of the *c* axis ("handle" bonds), are just slightly shorter than the As1−Cd1 bonds in the *ab* plane ("rib" bonds), 2.6385(14) Å vs 2.6494(6) Å, respectively. These Cd−As distances are shorter than the Cd−As distances in $Ba_2Cd_2As_3$ (2.715−2.909 Å),[16] in $BaCd_2As_2$ (2.737−2.814 Å),[38] and in KCdAs (2.725 Å).[39]

As discussed by Hoffmann et al. in an earlier publication,[40] this is a prominent structural feature, and the "handle" bond should be shorter than the "rib" bonds only when the transition metal has half-filled d bands; for filled d bands as in Cd, on the basis of the same theoretical analyses, one should expect the "handle" bond to be longer than the "rib" bonds, just as in $CaCd_2As_2$ (d^{handle}_{Cd-As} = 2.837 Å vs d^{rib}_{Cd-As} = 2.698 Å, respectively).[40] This apparent violation of the rules is likely due to the "dimerization" of the $^2_\infty[Cd_2As_2]^{2-}$ layers here (Figure 2), which leaves the As atom in middle of the $^2_\infty[Cd_4As_3]^-$ slab, As2, with a distinctly different local environment. This site has eight Cd neighbors in a distorted cubic fashion, with two sets of Cd−As2 contacts—one in a direction of the *c* axis (Cd1−As2) with a distance of 3.1947(13) Å and the other one, i.e., the Cd2−As2 bond, which measures 2.8250(6) Å. Both bonds are longer (weaker) than the Cd−As1 interactions, due to the increased coordination number (CN) of As2. Such long distances signify interactions, which are weakly bonding, in agreement with the electronic calculations (*vide infra*). Here, we specifically mention that eight-coordinated As atoms are not typically seen in Zintl compounds.[41] There are precedents for arsenic in such an unusual coordination in some

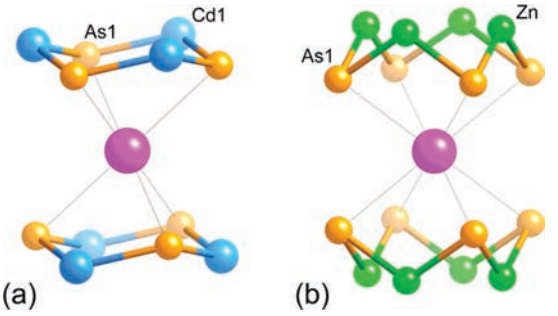

Figure 3. Cation coordination polyhedra in $RbCd_4As_3$ (a) and $RbZn_4As_3$ (b). The first and second coordination spheres (distances up to 4.2 Å) are shown.

metal-rich arsenides—$Ru_2Fe_{10}As_5$[42] and Cr_4As_3[43] are reported with the same coordination numbers; $BaNi_9As_5$ can be cited as a rare example of nine-coordinated As.[44] The transition-metal-rich compounds $EuNi_5As_3$[44] and $DyNi_4As_2$[45] are reported with As in cubic holes, although the description given therein includes the second coordination spheres as well. The As atoms in the binary phase Cd_3As_2[25] are six-bonded, with average Cd−As distances comparable with the length of the As2−Cd2 bond in $RbCd_4As_3$. Nonetheless, these are not examples with directional interactions involving As.

The alkali-metal cation resides in an octahedron of six As atoms, with a Rb−As distance of 3.5108(9) Å. At a longer distance, 3.9311(10) Å, there are six Cd atoms in the second coordination sphere, which together with the As atoms form two heteroatomic six-membered rings in a chair-like conformation around Rb (Figure 3).

$RbZn_4As_3$, as mentioned previously, crystallizes with the tetragonal space group *P*4/*mmm* (No. 123, *Z* = 1) and is isostructural to the known compounds KCu_4S_3 and $BaMg_4Si_3$ (Pearson symbol *tP*8).[21,46] The other members of this series include

dx.doi.org/10.1021/ic2009418 |*Inorg. Chem.* 2011, 50, 8375–8383

KZn_4As_3, $CsZn_4As_3$, $CsCd_4As_3$ (the only Cd-based compound here), $CsZn_4P_3$, and $RbZn_4P_3$. The $RbZn_4As_3$ structure contains four crystallographically independent atoms, one Rb, one Zn, and two As, and could be rationalized as polyanionic layers $^2_\infty[Zn_4As_3]^-$, separated and charge-balanced by Rb^+ cations (Figure 4). The $^2_\infty[Zn_4As_3]^-$ layers are based on $ZnAs_4$ tetrahedra, which are condensed by edge-sharing in the *ab* plane and stacked along the *c*-crystallographic direction. The Zn site is at the center of a slightly distorted As tetrahedron with As−Zn−As angles in the range of 103.38(2)° to 113.04(3)° (Table 3). Zn−As bonding distances are 2.5006(5) Å and 2.6580(5) Å, matching reasonably closely the sum of Zn and As covalent radii (r_{Zn} = 1.22 Å; r_{As} = 1.21 Å)[36] and comparing well with the corresponding distances found in Zintl compounds such as Ba_2ZnAs_2 (r_{Zn-As} = 2.592 Å),[12] $BaZn_2As_2$ (r_{Zn-As} = 2.573 Å),[47] and $Eu_{11}Zn_6As_{12}$ (r_{Zn-As} = 2.455−2.575 Å),[48] among others. The two different As sites have different local environments—As1 is four-coordinated and can be viewed as occupying a capping position of the Zn square plane (in alternating manner), much like the As atoms in the PbO-type $^2_\infty[Fe_2As_2]^-$ layers in $RbFe_2As_2$.[3] As2, on the other hand, is bonded to eight Zn atoms in a cubic arrangement (similar to As2 in $RbCd_4As_3$), with an As2−Zn distance longer than that between the four-coordinated As1 and Zn (Table 3). The CN8 for As2 can be again explained by the imaginary "dimerization" of $^2_\infty[Zn_2As_2]^{2-}$ layers with the PbO-like topology,[21] which leaves the As2 atom positioned between two adjacent Zn square nets (Figure 2).

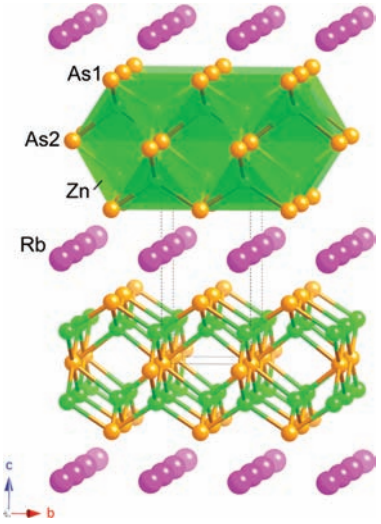

Figure 4. Combined ball-and-stick and polyhedral representations of the crystal structure of $RbZn_4As_3$. Rb atoms are shown as magenta spheres. Zn and As atoms are shown as green and tangerine spheres, respectively. Zn−As bonds are highlighted and the unit cell is outlined.

Compared with $RbCd_4As_3$, the Rb^+ cation in $RbZn_4As_3$ has a very different environment. In the $RbZn_4As_3$ structure, the Rb^+ cation is found in a cubic hole of eight As1 anions, which are positioned 3.6503(6) Å away (Table 3). The second coordination sphere is made up of eight Zn atoms at a distance of 4.1001(9) Å (Figure 3). Emphasizing the covalent Zn−As interactions, Rb^+ could be considered as being sandwiched between two eight-membered rings of Zn_4As_4. If the very distant As2 atoms are also considered, the 18-vertex Zn/As arrangement around Rb resembles the shape of the von Fedorov polyhedron, commonly observed in the $BaAl_4$-type structures.[49] Such a local environment of the alkali-metal in $RbZn_4As_3$ is very different from $RbCd_4As_3$ (*vide supra*), where the lower coordination number accounts for the closer-packed configuration (recall that d_{Rb-As} = 3.5108(9) Å). Since both compounds are isoelectronic, geometric (crystal packing) considerations, most likely, are the decisive factor that governs their formation. Further analyses and discussion on the differences between the rhombohedral and tetragonal systems are given in the following two paragraphs.

Having discussed the important structural characteristics of both $RbCd_4As_3$ and $RbZn_4As_3$ structures, we briefly turn our attention to the topological relationships between the structures in question and those of two of the most ubiquitous structure types among the intermetallic compounds. A schematic representation that illustrates the genealogy of $RbCd_4As_3$ from the hypothetical $RbCd_2As_2$ phase ($CaAl_2Si_2$ type),[21] and of $RbZn_4As_3$ from the hypothetical $RbZn_2As_2$ phase ($CeAl_2Ga_2$/$ThCr_2Si_2$ type)[21] is shown in Figure 2. As seen from the figure, the relationships are easily recognizable by comparing the diagrams on the left and the right sides—to form the $^2_\infty[Cd_4As_3]^-$ layer in $RbCd_4As_3$, one must fuse two neighboring $^2_\infty[Cd_2As_2]^{2-}$ layers by sharing the As atoms from the bottom of the upper layer and the As atoms from the top of the lower layer and removing the spacer Rb^+ cations, which separate the slabs. The same two-dimensional motifs may also be derived by splitting (reducing) the imaginary CdAs network with the wurtzite-type, followed by a subsequent reconstruction and

Table 4. Pauling's Metallic Radii (Å), *A*−*A* Distances (Å), Cd/Zn−*Pn* Distances (Å), and Their Ratios for the Compounds from Each Family (*A* = Cs, Rb, K, Na, *Pn* = As, P)

rhombohedral series	$RbCd_4As_3$	KCd_4As_3	$NaCd_4As_3$	$NaZn_4As_3$	KZn_4P_3	KCd_4P_3
r_A	2.16	2.025	1.572	1.572	2.025	2.025
$d_{Cd/Zn-Pn}$	2.649	2.648	2.636	2.459	2.376	2.562
d_{A-A}	4.475	4.471	4.455	4.169	4.045	4.353
$d_{A-A}/d_{Cd/Zn-Pn}$	1.689	1.688	1.690	1.695	1.702	1.699
tetragonal series	$CsCd_4As_3$	$CsZn_4As_3$	$RbZn_4As_3$	$CsZn_4P_3$	$RbZn_4P_3$	KZn_4As_3[a]
r_A	2.35	2.35	2.16	2.35	2.16	2.025
$d_{Cd/Zn-Pn}$	2.699	2.494	2.501	2.413	2.408	2.479
d_{A-A}	4.500	4.179	4.171	4.085	4.060	4.154
$d_{A-A}/d_{Cd/Zn-Pn}$	1.667	1.676	1.668	1.693	1.686	1.676

[a] Because of the inability to obtain single crystals, the values for KZn_4As_3 have been estimated from unit cell constants obtained from powder X-ray diffraction data and atomic coordinates taken from $RbZn_4As_3$.

dx.doi.org/10.1021/ic2009418 |*Inorg. Chem.* 2011, 50, 8375–8383

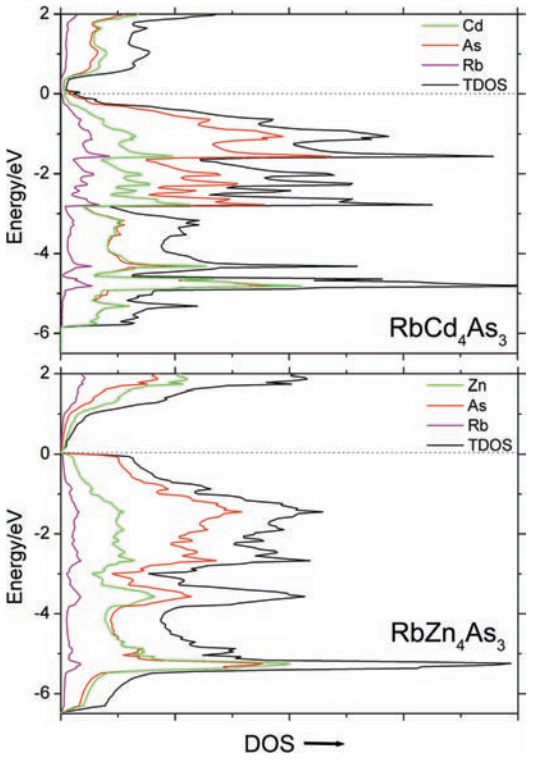

Figure 5. Total and partial DOS diagrams for $RbCd_4As_3$ and $RbZn_4As_3$. Total DOS (solid black line), Rb partial DOS (purple), Cd/Zn partial DOS (green), and As partial DOS (red) are plotted. E_F (dotted line) is set as the energy reference (0 eV).

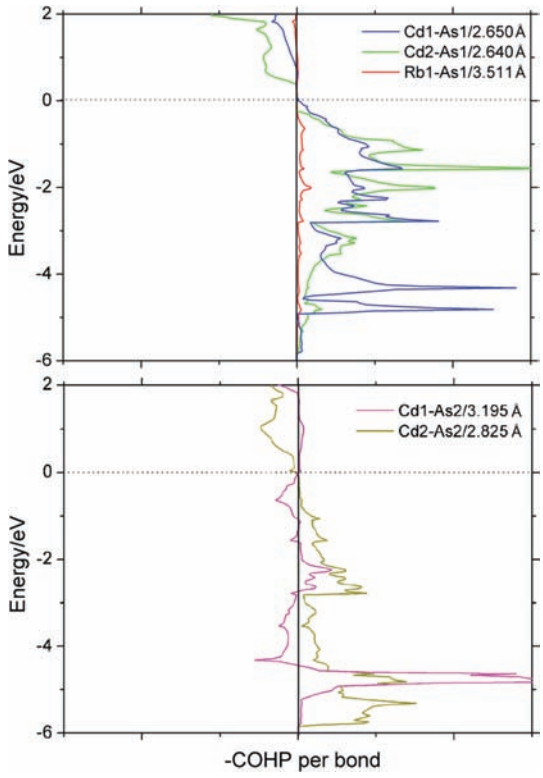

Figure 6. COHP curves for the average Cd−As and Rb−As interactions in $RbCd_4As_3$. In the COHP curves, the positive values (right) indicate bonding interactions; the negative values (left) indicate antibonding interactions.

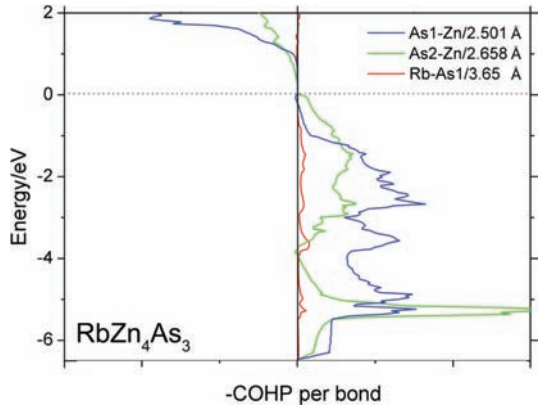

Figure 7. COHP curves for the average Zn−As and Rb−As interactions in $RbZn_4As_3$. In the COHP curves, the positive values (right) indicate bonding interactions; the negative values (left) indicate antibonding interactions.

insertion of spacer Rb^+ cations. The "formation" of the $RbZn_4As_3$ structure from the imaginary $RbZn_2As_2$ with the $ThCr_2Si_2$ type proceeds through similar condensation of neighboring $^2_\infty[Zn_2As_2]^{2-}$ layers, concomitant with the elimination of layers with alkali metals.

Once these close relationships with the two common structure types are realized, one could attempt to explain the occurrence of almost all Cd-containing compounds in the rhombohedral structure, while the Zn-containing compounds are more prone to form with the tetragonal structure. This is a logical starting point because there is already considerable information on the chemical bonding in compounds with similar bonding characteristics.[40,49] Surveying the literature readily shows that a simple generalization would have been possible if the electron counts in both cases were different—after all, it is well-known that most $CaAl_2Si_2$-like compounds are closed-shell 16-electron/f.u. systems,[40,49] while the compounds with the $CeAl_2Ga_2$/$ThCr_2Si_2$ ($BaAl_4$) type structure favor 12−14 electrons per f.u.[40,49] However, that is not the case with $RbCd_4As_3$ and $RbZn_4As_3$, as the formal electron count in both structures is the same—electronic structure calculations for both (*vide infra*) show the characteristics of the charge-balanced valence compounds, i.e., the semiconductors and the Zintl phases. An explanation involving the different electronegativities of Zn and Cd is also unlikely, since both $CsCd_4As_3$ and $CsZn_4As_3$ form with the same structure as $RbZn_4As_3$. Using parallels with pairs of compounds such as $Sr_{21}Cd_4Bi_{18}$ and $Ba_{21}Cd_4Sb_{18}$,[11] $SrMn_2Pn_2$ and $BaMn_2Pn_2$ (Pn = P, Sb),[50] or $CaGa_2As_2$ and $SrGa_2As_2$,[51] which are isoelectronic but not isostructural, we can speculate that structure selections are governed by the cation and anion spatial requirements. For example, the optimal balance between the cation and anion sizes in the tetragonal $RbZn_4As_3$ structure would be achieved if large cations were used, which would allow them to be effectively enclosed between the eight-membered rings of two neighboring $^2_\infty[Zn_4As_3]^-$ layers (Figure 3). Of course, large is a relative term since the size of the cations' holes is a structural parameter that is closely related to the Cd−As and Zn−As distances as well. Therefore, we can argue that the Rb^+ cations are unable to stabilize tetragonal $RbCd_4As_3$, which forms

dx.doi.org/10.1021/ic2009418 |*Inorg. Chem.* 2011, 50, 8375–8383

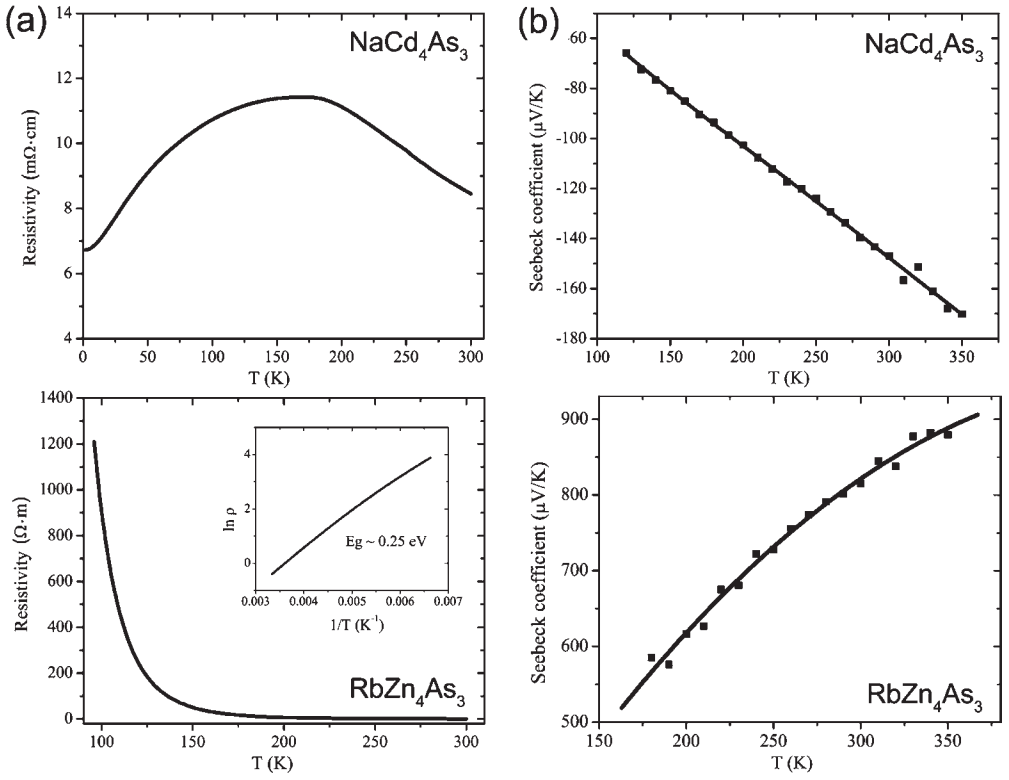

Figure 8. Electrical resistivity $\rho(T)$ (a) and Seebeck coefficient $S(T)$ (b) of $NaCd_4As_3$ and $RbZn_4As_3$, both measured on polycrystalline pellets.

with the energetically more favorable rhombohedral arrangement, where the octahedral holes between neighboring $^2_\infty[Cd_4As_3]^-$ layers (Figure 3) would be preferred. Such reasoning also helps one to understand the occurrence of $CsCd_4As_3$, $CsZn_4As_3$, and $RbZn_4P_3$ as tetragonal phases, while $NaCd_4As_3$, $NaZn_4As_3$, and KZn_4P_3 are with the rhombohedral structure (Table 4).

Bonding and Electronic Structure. TB-LMTO-ASA electronic band structure calculations were done for both $RbCd_4As_3$ and $RbZn_4As_3$. The plots of density of states (DOS) are projected in Figure 5; the crystal orbital Hamilton populations (COHP) for selected atom pairs are presented in Figures 6 and 7. As shown in the DOS plot of $RbCd_4As_3$, a small overlap between the top of the valence band and the bottom of the conduction band is noticeable, suggesting it to be a semimetal. On the other hand, the DOS diagram for $RbZn_4As_3$ shows a clearer band gap, indicating that the compound would be an intrinsic semiconductor, albeit with a very small band gap. However, on the basis of the well-known fact that LMTO calculations usually underestimate the band gap, these calculations have to be considered cautiously and should be verified experimentally. Regrettably, because of the inadequate size of the single crystals of $RbCd_4As_3$ and $RbZn_4As_3$, we were unable to carry out quantitative resistivity measurements on these samples; the reported data on polycrystalline pellets (*vide infra*) serve only as a qualitative proof-of-principle.

The states just below the Fermi levels in both compounds, from −3 to 0 eV, are predominately from the contribution of the As p orbitals, as well as the contribution from the Cd p or Zn p orbitals, suggesting that the polyanionic substructure plays the most important role in determining the transport properties of the compound. However, the small contribution from the Rb is also noticeable in both compounds. Although it is insignificant compared with the total DOS, the overlap between the Rb states and those from the polyanionic substructure becomes the dominant factor in selecting structure types, as we have discussed previously. From −3 eV down to −5 eV, the states could be attributed to the admixture of As p and Cd s or Zn s states. Well below that energy are found the filled Cd d or Zn d orbitals and the As 4s lone pairs.

The COHP diagrams of the Cd−As interactions show that the "normal" (shorter) bonds signify nearly optimized bonding at the Fermi level (Figure 6). The elongated distance between As2 and Cd1 (3.195 Å), as mentioned earlier, suggests weak bonding between these two atoms, and indeed, the COHP for As2−Cd1 has an antibonding character just below the Fermi level (Figure 6). This weakening effect is compensated by the strong bonding between As1−Cd1, As1−Cd2, and As2−Cd2, making the overall structure energetically stable. In the case of $RbZn_4As_3$, both As1−Zn and As2−Zn interactions are fully optimized at the Fermi level (Figure 7), which is a typical feature for the anionic substructure in Zintl compounds.[9] The Rb−As interactions mostly are ionic in character and fully optimized for both $RbCd_4As_3$ and $RbZn_4As_3$. The mostly electrostatic nature of the Rb−As interactions, which is consistent with the Zintl formalism, results in very small integrated COHP values for the average Rb−As pairs, compared with the average Cd−As or Zn−As interactions.

Properties. The electrical resistivity and Seebeck coefficient of $NaCd_4As_3$, measured on polycrystalline pellets, are presented in Figure 8. $NaCd_4As_3$, instead of $RbCd_4As_3$, was chosen for the measurements because the latter was always contaminated with $Rb_2Cd_5As_4$.[23] As shown in the figure, the resistivity does not change much in the temperature range of 5−300 K, with a room

dx.doi.org/10.1021/ic2009418 |*Inorg. Chem.* 2011, 50, 8375–8383

temperature ρ of about 9 m$\Omega\cdot$cm. From 5 to 180 K, the resistivity increases slowly with the increasing temperature, in agreement with the expected behavior for a degenerate semiconductor. The decrease in resistivity above 180 K is most likely due to the intrinsic excitation of $NaCd_4As_3$, as expected for a typical semiconductor. Similar conducting behavior has already been seen and discussed for the polycrystalline pellets of the compounds of $CaZn_2Sb_2$,[7] $BaZn_2Sb_2$,[52] and $EuCd_2Sb_2$.[53] The Seebeck coefficient shows negative values in the whole temperature range, indicating the electrons as the dominant charge carriers. The absolute values increase linearly as the temperature increases, reaching a promising value of 170 μV/K at 350 K. Since $RbCd_4As_3$ is isoelectronic and isostructural to $NaCd_4As_3$, it is expected that it will have similar charge-transport properties. On the basis of the above, the compounds from this family could be promising thermoelectric materials, provided their thermal conductivity is low.[54]

Measurements on a polycrystalline pellet of $RbZn_4As_3$ were also conducted. Unlike $NaCd_4As_3$, the resistivity of $RbZn_4As_3$ increases exponentially as the temperature decreases, suggesting typical semiconductor behavior, which is consistent with the band structure calculation. The room temperature resistivity is quite high though, about 100 $\Omega\cdot$cm, and the Seebeck coefficient at room temperature is very large, about 800 μV/K. This could be due to oxidized insulating regions that are formed on the surface or inside the specimen and/or grain boundaries. We had previously seen such anomalously high resistivity for single crystals of $Ba_2Cd_2As_3$, where the results were reproducible for different batches, yet, in an apparent disagreement with the computed band gap.[16] It is certainly possible that a measurement procedure, which does not require the sample to be removed from the inert atmosphere glovebox, would provide a more accurate estimate of the resistivity of this material. The positive slope of the Seebeck coefficient's dependence on the temperature suggests holes as the dominant charge carriers in this compound. We would expect similar transport properties for other compounds with the tetragonal structure. Obviously, the high resistivity of the compounds of this family would eliminate the possibility for them as being efficient thermoelectric materials.

CONCLUSIONS

Twelve new Zintl compounds, ACd_4Pn_3 and AZn_4Pn_3 (A = Cs, Rb, K, Na, Pn = As, P), have been synthesized and structurally characterized. The Cd-containing compounds tend to crystallize with a new rhombohedral structure with space group $R\bar{3}m$ (No. 166), while the Zn-containing compounds prefer the tetragonal KCu_4S_3 structure with space group $P4/mmm$. Such structure preference could be linked to the cation size and the packing efficiency. The close structural relationships to the $CaAl_2Si_2$ and $ThCr_2Si_2$ structure types may indicate similar crystal chemistry, such as amenability for chemical substitution. The transport property measurements on $NaCd_4As_3$ show a favorable combination of electrical conductivity and Seebeck coefficient, which suggest that the compounds of this family could be promising thermoelectric materials.

ASSOCIATED CONTENT

Supporting Information. A combined X-ray crystallographic file in CIF format (within a ZIP file), tables with crystallographic information for all structurally characterized compounds, plots of the crystal structures with anisotropic displacement parameters, and a representative powder X-ray diffraction pattern for $RbZn_4As_3$. This material is available free of charge via the Internet at http://pubs.acs.org.

AUTHOR INFORMATION

Corresponding Author

*Phone: (302) 831-8720. Fax: (302) 831-6335. E-mail: bobev@udel.edu.

ACKNOWLEDGMENT

S.B. acknowledges financial support from the U.S. Department of Energy through a grant (DE-SC0001360).

REFERENCES

(1) (a) Kleinke, H. *Chem. Mater.* **2010**, *22*, 604–611. (b) Sootsman, J. R.; Chung, D. Y.; Kanatzidis, M. G. *Angew. Chem., Int. Ed.* **2009**, *48*, 8616–8639. (c) Ishida, K.; Nakaii, Y.; Hosono, H. *J. Phys. Soc. Jpn.* **2009**, *78*, 062001. (d) Yang, W. L.; Sorini, A. P.; Chen, C.-C.; Moritz, B.; Lee, W.-S.; Vernay, F.; Olalde-Velasco, P.; Denlinger, J. D.; Delley, B.; Chu, J.-H.; Analytis, J. G.; Fisher, I. R.; Ren, Z. A.; Yang, J.; Lu, W.; Zhao, Z. X.; van den Brink, J.; Hussain, Z.; Shen, Z.-X.; Devereaux, T. P. *Phys. Rev. B* **2009**, *80*, 014508.

(2) (a) Kamihara, Y.; Watanabe, T.; Hirano, M.; Hosono, H. *J. Am. Chem. Soc.* **2008**, *130*, 3296–3297. (b) Takahashi, H.; Igawa, K.; Arii, K.; Kamihara, Y.; Hirano, M.; Hosono, H. *Nature* **2008**, *453*, 376–378. (c) Ren, Z. A.; Yang, J.; Lu, W.; Yi, W.; Che, G. C.; Dong, X. L.; Sun, L. L.; Zhao, Z. X. *Mater. Res. Innovat.* **2008**, *12*, 105–106. (d) Ren, Z. A.; Che, G. C.; Dong, X. L.; Yang, J.; Lu, W.; Yi, W.; Shen, X. L.; Li, Z. C.; Sun, L. L.; Zhou, F.; Zhao, Z. X. *EPL* **2008**, *83*, 17002.

(3) (a) Christianson, A. D.; Goremychkin, E. A.; Osborn, R.; Rosenkranz, S.; Lumsden, M. D.; Malliakas, C. D.; Todorov, I. S.; Claus, H.; Chung, D. Y.; Kanatzidis, M. G.; Bewley, R. I.; Guidi, T. *Nature* **2008**, *456*, 930–932. (b) Sasmal, K.; Lv, B.; Lorenz, B.; Guloy, A. M.; Chen, F.; Xue, Y. Y.; Chu, C. W. *Phys. Rev. Lett.* **2008**, *101*, 107007. (c) Rotter, M.; Tegel, M.; Johrendt, D. *Phys. Rev. Lett.* **2008**, *101*, 107006.

(4) (a) Parker, D. R.; Pitcher, M. J.; Baker, P. J.; Franke, I.; Lancaster, T.; Blundell, S. J.; Clarke, S. J. *Chem. Commun.* **2009**, *16*, 2189–2191. (b) Tapp, J. H.; Tang, Z. J.; Lv, B.; Sasmal, K.; Lorenz, B.; Chu, P. C. W.; Guloy, A. M. *Phys. Rev. B* **2008**, *78*, 060505. (c) Chu, C. W.; Chen, F.; Gooch, M.; Guloy, A. M.; Lorenz, B.; Lv, B.; Sasmal, K.; Tang, Z. J.; Tapp, J. H.; Xue, Y. Y. *Physica C* **2009**, *469*, 326–331.

(5) Brown, S. R.; Kauzlarich, S. M.; Gascoin, F.; Snyder, G. J. *Chem. Mater.* **2006**, *18*, 1873–1877.

(6) Sales, B. C.; Mandrus, D.; Williams, R. K. *Science* **1996**, *272*, 1325–1328.

(7) Gascoin, F.; Ottensmann, S.; Stark, D.; Haïle, S. M.; Snyder, G. J. *Adv. Funct. Mater.* **2005**, *15*, 1860–1864.

(8) Zhang, H.; Zhao, J.-T.; Grin, Y.; Wang, X.-J.; Tang, M.-B.; Man, Z.-Y.; Chen, H.-H.; Yang, X.-X. *J. Chem. Phys.* **2008**, *129*, 164713.

(9) (a) Guloy, A. M. Polar Intermetallics and Zintl Phases along the Zintl Border. In *Inorganic Chemistry in Focus III*; Wiley-VCH Verlag GmbH & Co. KGaA: Weinheim, Germany, 2006. (b) Kauzlarich, S. M. *Chemistry, Structure and Bonding of Zintl Phases and Ions*; VCH Publishers: New York, 1996 and the references therein.

(10) (a) Alemany, P.; Llunell, M.; Canadell, E. *Inorg. Chem.* **2006**, *45*, 7235–7241. (b) Gallup, R. F.; Fong, C. Y.; Kauzlarich, S. M. *Inorg. Chem.* **1992**, *31*, 115–118. (c) Young, D. M.; Torardi, C. C.; Olmstead, M. M.; Kauzlarich, S. M. *Chem. Mater.* **1995**, *7*, 93–101.

(11) Xia, S.-Q.; Bobev, S. *Inorg. Chem.* **2008**, *47*, 1919–1921.

(12) Saparov, B.; Bobev, S. *Inorg. Chem.* **2010**, *49*, 5173–5179.

(13) (a) Saparov, B.; Bobev, S.; Ozbay, A; Nowak, E. R. *J. Solid State Chem.* **2008**, *181*, 2690–2696. (b) Xia, S.-Q.; Bobev, S. *J. Comput. Chem.* **2008**, *29*, 2125–2133.
(14) (a) Bobev, S.; Thompson, J. D.; Sarrao, J. L.; Olmstead, M. M.; Hope, H.; Kauzlarich, S. M. *Inorg. Chem.* **2004**, *43*, 5044–5052. (b) Xia, S.-Q.; Bobev, S. *J. Am. Chem. Soc.* **2007**, *129*, 10011–10018.
(15) Xia, S.-Q.; Bobev, S. *J. Am. Chem. Soc.* **2007**, *129*, 4049–4057.
(16) Saparov, B.; He, H.; Zhang, X.; Greene, R.; Bobev, S. *Dalton Trans.* **2010**, *39*, 1063–1070.
(17) Saparov, B.; Xia, S.-Q.; Bobev, S. *Inorg. Chem.* **2008**, *47*, 11237–11244.
(18) Saparov, B.; Broda, M.; Ramanujachary, K. V.; Bobev, S. *Polyhedron* **2010**, *29*, 456–462.
(19) Saparov, B.; Saito, M.; Bobev, S. *J. Solid State Chem.* **2011**, *184*, 432–440.
(20) (a) Andersen, O. K. *Phys. Rev. B* **1975**, *12*, 3060–3083. (b) Andersen, O. K.; Jepsen, O. *Phys. Rev. Lett.* **1984**, *53*, 2571–2574. (c) Andersen, O. K.; Pawlowska, Z.; Jepsen, O. *Phys. Rev. B* **1986**, *34*, 5253–5269.(d) Skriver, H. L. *The LMTO Method*; Springer: Berlin, 1984.
(21) Villars, P.; Calvert, L. D. *Pearson's Handbook of Crystallographic Data for Intermetallic Phases*, 2nd ed.; American Society for Metals: Materials Park, OH, 1991.
(22) Liu, Y.; Wu, L.-M.; Li, L.-H.; Du, S.-W.; Corbett, J. D.; Chen, L. *Angew. Chem., Int. Ed.* **2009**, *48*, 5305–5308.
(23) He, H.; Bobev, S. Unpublished results: $Rb_8Zn_{18}As_{28}$ in $Pm\bar{3}n$, $a = 10.7413(6)$ Å (isostructural to $Cs_8Zn_{18}Sb_{28}$ in ref 21); $Rb_2Cd_5As_4$ in *Cmcm*, $a = 12.432(4)$ Å, $b = 7.587(3)$ Å, $c = 12.507(4)$ Å (isostructural to $Cs_2Cd_5Sb_4$ in ref 22).
(24) Cervinka, L.; Hruby, A. *Acta Crystallogr.* **1970**, *26B*, 457–458.
(25) Weglowski, S.; Lukaszewicz, K. *Bull. Acad. Polon. Sci., Ser. Sci. Chim.* **1968**, *16*, 177–182.
(26) (a) *SMART NT*, version 5.63; Bruker Analytical X-ray Systems, Inc.: Madison, WI, 2003. (b) *SAINT NT*, version 6.45; Bruker Analytical X-ray Systems, Inc.: Madison, WI, 2003.
(27) *SADABS NT*, version 2.10; Bruker Analytical X-ray Systems, Inc.: Madison, WI, 2001.
(28) *SHELXTL*, version 6.12; Bruker Analytical X-ray Systems, Inc.: Madison, WI, 2001.
(29) Gelato, L. M.; Parthe, E. *J. Appl. Crystallogr.* **1987**, *20*, 139–146.
(30) Jepsen, O.; Andersen, O. K. *TB-LMTO-ASA Program*, version 4.7; Max-Planck-Institut für Festkörperforschung: Stuttgart, Germany, 1998.
(31) von Barth, U.; Hedin, L. *J. Phys. C: Solid State Phys.* **1972**, *5*, 1629–1642.
(32) Koelling, D. D.; Harmon, B. N. *J. Phys. C: Solid State Phys.* **1977**, *10*, 3107–3114.
(33) Lambrecht, W. R. L.; Andersen, O. K. *Phys. Rev. B: Condens. Matter.* **1986**, *34*, 2439–2449.
(34) Blöchl, P. E.; Jepsen, O.; Andersen, O. K. *Phys. Rev. B: Condens. Matter.* **1994**, *49*, 16223–16233.
(35) *ICSD Database*; Fachinformationszentrum: Karlsruhe, Germany, 2010.
(36) Pauling, L. *The Nature of the Chemical Bond*; Cornell University Press: Ithaca, NY, 1960.
(37) Klüfers, P.; Mewis, A. *Z. Naturforsch.* **1977**, *32b*, 753–756.
(38) Klüfers, P.; Mewis, A. *Z. Kristallogr.* **1984**, *169*, 135–147.
(39) Kahlert, H.; Schuster, H. U. *Z. Naturforsch.* **1976**, *31b*, 1538–1539.
(40) (a) Zheng, C.; Hoffmann, R.; Nesper, R.; von Schnering, H.-G. *J. Am. Chem. Soc.* **1986**, *108*, 1876–1884. (b) Burdett, J. K.; Miller, G. J. *Chem. Mater.* **1990**, *2*, 12.
(41) $RbCd_4As_3$ and $RbZn_4As_3$ are Zintl phases, as confirmed through the electronic structure calculations. Following the Zintl formalism, both structures can be rationalized as polyanionic layers based on covalent Cd—As or Zn—As bonds and Rb^+ cations, i.e., $Rb^+[Cd_4As_3]^-$ and $Rb^+[Zn_4As_3]^-$, respectively. Exaggerating the ionicity of the Cd—As or Zn—As interactions and assigning oxidation numbers leads to $(Rb^+(Cd^{2+})_4(As^{3-})_3$ and $Rb^+(Zn^{2+})_4(As^{3-})_3)$, respectively.
(42) Maaref, S.; Madar, R.; Chaudouet, P.; Fruchart, R.; Senateur, J. P.; Averbuch-Pouchot, M. T.; Bacmann, M.; Durif, A.; Wolfers, P. *Mater. Res. Bull.* **1983**, *18*, 473–480.
(43) Baurecht, H. E.; Boller, H.; Nowotny, H. N. *Monatsh. Chem.* **1970**, *101*, 1696–1703.
(44) Probst, H.; Mewis, A. *Z. Anorg. Allg. Chem.* **1991**, *597*, 173–182.
(45) Jeitschko, W.; Terbuechte, L. J.; Reinbold, E. J.; Pollmeier, P. G.; Vomhof, T. *J. Less-Common Met.* **1990**, *161*, 125–134.
(46) $BaMg_4Si_3$ (Zürcher, F.; Wengert, S.; Nesper, R. *Inorg. Chem.* **1999**, *38*, 4567–4569) forms with the same space group as $RbZn_4As_3$, and with the same Wyckoff sequence—*a b h i*. However, in $RbZn_4As_3$, the *c*/*a* ratio is 2.48 (layered arrangement), whereas in $BaMg_4Si_3$ $c/a = 1.48$ (Mg—Si framework with Si—Si bonds). Hence, the two structures should not be considered isotypic.
(47) Hellmann, A.; Loehken, A.; Wurth, A.; Mewis, A. *Z. Naturforsch.* **2007**, *62b*, 155–161.
(48) Saparov, B.; Bobev, S. *Acta Crystallogr.* **2010**, *E66*, i24.
(49) Zheng, C.; Hoffmann, R. *J. Solid State Chem.* **1988**, *72*, 58–71.
(50) (a) Brock, S. L.; Greedan, J. E.; Kauzlarich, S. M. *J. Solid State Chem.* **1994**, *109*, 416–418. (b) Xia, S.-Q.; Myers, C.; Bobev, S. *Eur. J. Inorg. Chem.* **2008**, 4262–4269.
(51) He, H.; Stearrett, R.; Nowak, E. R.; Bobev, S. *Eur. J. Inorg. Chem.* **2011**, DOI: 10.1002/ejic.201100065.
(52) Wang, X.-J.; Tang, M.-B.; Zhao, J.-T.; Chen, H.-H.; Yang, X.-X. *Appl. Phys. Lett.* **2007**, *90*, 232107.
(53) Zhang, H.; Baitinger, M.; Tang, M.-B.; Man, Z.-Y.; Chen, H.-H.; Yang, X.-X.; Liu, Y.; Chen, L.; Grin, Y.; Zhang, J.-T. *Dalton Trans.* **2010**, *39*, 1101–1104.
(54) Rowe, D. M. *CRC Handbook of Thermoelectrics*; CRC Press: New York, 1995.